JGR Space Physics

RESEARCH ARTICLE
10.1029/2019JA027535

# VIPIR and 50 MHz Radar Studies of Gravity Wave Signatures in 150-km Echoes Observed at Jicamarca

**Pablo M. Reyes[1,2], Erhan Kudeki[1], Gerald A. Lehmacher[3], Jorge L. Chau[4], and Marco A. Milla[5]**

[1]Department of Electrical and Computer Engineering, University of Illinois at Urbana-Champaign, Champaign, IL, USA, [2]Now at Center for Geospace Studies, SRI International, Menlo Park, CA, USA, [3]Department of Physics and Astronomy, Clemson University, Clemson, SC, USA, [4]Department of Radar Remote Sensing, Leibniz Institute of Atmospheric Physics, Kühlungsborn, Germany, [5]Radio Observatorio de Jicamarca, Instituto Geofísico del Perú, Lima, Peru

**Key Points:**
- VIPIR ionosonde and 50 MHz radar data are used jointly to investigate the equatorial 150-km irregularities
- The 150-km echo layers seen in 50 MHz data are aligned with VIPIR isodensity contours in the region rippled by gravity wave modulations
- The 150-km irregularity models need to account for gravity wave modulation and forcing effects

**Correspondence to:**
E. Kudeki,
erhan@illinois.edu

**Citation:**
Reyes, P. M., Kudeki, E., Lehmacher, G. A., Chau, J. L., & Milla, M. A. (2020). VIPIR and 50 MHz radar studies of gravity wave signatures in 150-km echoes observed at Jicamarca. *Journal of Geophysical Research: Space Physics*, *125*, e2019JA027535. https://doi.org/10.1029/2019JA027535

Received 16 OCT 2019
Accepted 1 JUN 2020
Accepted article online 19 JUN 2020

**Abstract** Range-time-intensity (RTI) plots of 50 MHz radar backscatter detected at Jicamarca from the 150-km region of the equatorial ionosphere exhibit necklace-shaped multilayered structures first reported by Kudeki and Fawcett (1993, https://doi.org/10.1029/93GL01256). The backscatter layers also exhibit quasi-periodic intensity fluctuations with periods of about 5–15 min and are separated from adjacent layers by thin and undulating regions of no detectible power returns. A study of the fluctuating backscatter layers and undulating gap regions will be presented using VIPIR ionosonde data taken at the Jicamarca Radio Observatory simultaneously with high-resolution 50-MHz radar backscatter data. VIPIR virtual reflection height variations in time are noted to match the RTI gap-region undulations very closely at selected VIPIR frequencies (or, equivalently, electron densities at reflection heights). This matching enables assigning "true heights" to VIPIR virtual height contour maps, and a joint study of the contour maps with the 50-MHz radar RTI maps strongly suggests that correlated fluctuations and undulations observed in VIPIR and 50-MHz radar data are indicative of gravity wave-induced variations in the 150-km region ionosphere. Accordingly, a complete explanation of the 150-km echo phenomenon will need to include gravity wave coupling and forcing effects in the enhancement and suppression processes that can account for the observed fluctuations and gap-region features of necklace-shaped 150-km echo maps.

## 1. Introduction

The purpose of this paper is to present recent VIPIR ionosonde and 50-MHz radar backscatter data collected at the Jicamarca Radio Observatory (11.95°S, 76.87°W) that brings into focus the role played by gravity waves in the formation and modulations of 150-km equatorial radar echoes (e.g., Kudeki & Fawcett, 1993), a poorly understood phenomenon of the equatorial ionosphere despite some recent insights and progress (e.g., Oppenheim & Dimant, 2016). Figure 1 shows a Jicamarca range-time-intensity (RTI) map of the 50-MHz radar backscatter signal-to-noise ratio (SNR) from the equatorial ionosphere. The map includes a necklace-shaped structure centered about 150-km altitude representing intense radar returns. This structure is a permanent feature of daytime radar backscatter recordings at Jicamarca displaying a descending phase in the morning hours and an ascending phase in the afternoon. These so-called 150-km VHF echo signatures have also been observed at other equatorial and low-latitude locations (e.g., Brazil, India, and Pohnpei) (e.g., Kudeki et al., 1998; Patra et al., 2008; Patra & Rao, 2007, 2006; Rodrigues et al., 2011; Tsunoda & Ecklund, 2000, 2008; Yokoyama et al., 2009) and are therefore considered to be a ubiquitous feature of the low-latitude ionosphere.

Returning to Figure 1, the RTI map was constructed using 64-baud complementary coded pulse pairs with 1-μs bauds that resolve the slow fading mesospheric and 150-km echoes with a 150-m height resolution but fails to resolve with the same fidelity the fast fading signals scattered from the electrojet irregularities seen in Figure 1 as the bulky structure centered about 100-km altitude. Typical layer widths in the nicely resolved 150-km necklace structure are 5 to 10 km, and echo intensity within each layer exhibits temporal fluctuations with about 5- to 15-min period. Narrow "forbidden regions" separating adjacent echoing layers exhibit quasi-periodic height variations with also about 5- to 15-min periodicity. These features of the necklace-shaped 150-km echo RTI show relatively minor variations from day to day.

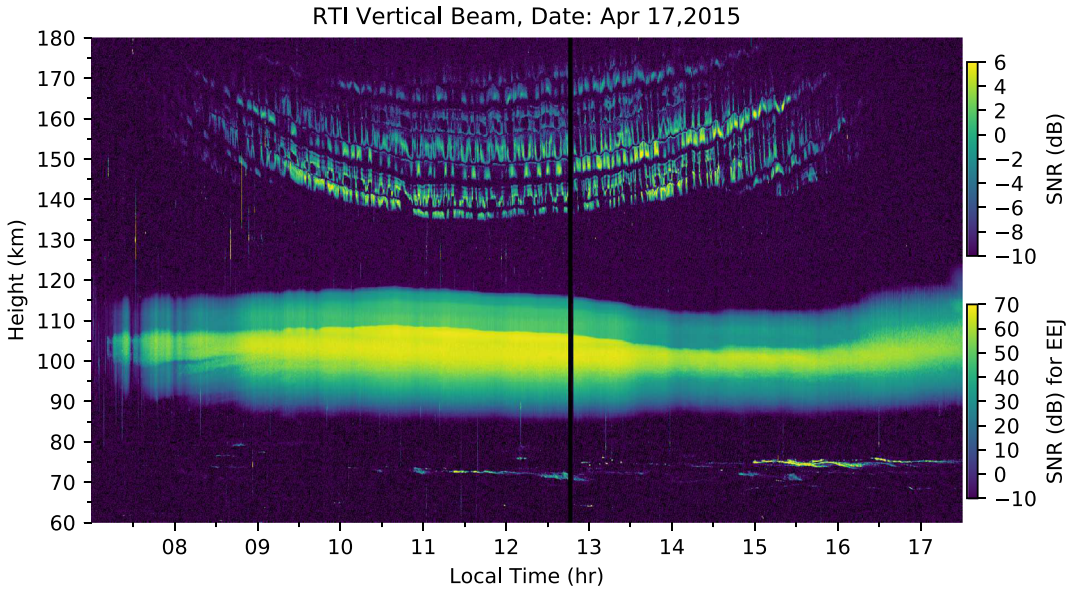


**Figure 1.** Range-time-intensity (RTI) plot of signal-to-noise ratio (SNR) of 50-MHz radar backscattering at JRO with a 150-m height resolution and a time resolution of about 8 s. The data used for this plot were taken during an MST-ISR-EEJ campaign at JRO. The RTI plot presents evidence for narrow scattering layers in the mesosphere (60–80 km), an oversaturated backscatter from the equatorial electrojet (90–120 km), and an intricately structured backscattered power pattern for the 150-km echoes (≥130 km), which is the subject of this study. Note that different color bars are used for electrojet returns and returns from mesosphere and 150-km region.

The 150-km echoes were initially noted and described by Balsley (1964) using oscilloscope screenshots and filmstrips as narrow stratified echoes showing simultaneously up to four layers at different heights in the region around 150 km of altitude. High-resolution recordings of these layers by Kudeki and Fawcett (1993) showed that the Doppler frequency shift of vertical incidence 150-km returns can be used to measure the vertical plasma drift velocities near the geomagnetic equator. The 150-km Doppler velocities are being routinely used at Jicamarca as a proxy for the **E×B** drift of the *F* region that drives the equatorial fountain effect (e.g., Chau & Woodman, 2004). More recently, Chau et al. (2009) and Chau and Kudeki (2013) discovered that the 150-km echoes consist of two distinct types, naturally enhanced incoherent scatter (NEIS) and scatter from field-aligned irregularities (FAIs), the former being the more abundant at Jicamarca. Even more recently, large-scale kinetic simulations of Oppenheim and Dimant (2016) have shown that energetic photoelectrons could be the cause of enhancement of plasma and ion line amplitudes around 150 km of altitude to cause enhanced backscatter from the region. Reyes (2012) studied the effects of solar flare events on the equatorial ionosphere and showed that the 150-km echoes were enhanced, obeying the increase in energetic solar flux (now contributing to the theory of the role of energetic photoelectrons in the enhance mechanism). The same study also observed that during solar flare events, distinct and neighboring layers of the 150-km echoes were compressed and pushed down during the onset of the flares.

In the present study we make use of joint Jicamarca observations conducted with the 50-MHz Jicamarca incoherent scatter radar (ISR) and a colocated VIPIR ionosonde system to advance our understanding of the physics of the 150-km echoing region. Both the ISR and VIPIR instruments were configured for high temporal and altitude resolution probing of the equatorial valley region ionosphere extending from the top of the equatorial electrojet (~110 km) to about 200 km height. High-resolution ISR and VIPIR records showed correlated fluctuations that will be analyzed in this paper in terms of plausible gravity wave-based models. The paper is organized as follows: In section 2 we provide descriptions of the instruments, the data sources, and present the pertinent data sets acquired using the 50-MHz Jicamarca ISR and the VIPIR ionosonde. Section 3describes the correlation observed between VIPIR virtual height oscillations and the fluctuations of 150-km echo layers seen in the ISR data. Finally, a discussion of the results and findings and our conclusions are presented in section 4.

**Table 1**
*Parameters for the MST Part of the MST-ISR-EEJ Experiment at Jicamarca*

| | |
|---|---|
| IPP | 202.5 km (1.35 ms) |
| Consecutive IPPs (burst)/coherent integrations | 20 |
| Bursts period/Doppler velocity range | (135 ms) / ±11.1 m/s |
| Complementary code | 64 bauds |
| Height resolution | 0.15 km |
| Transmitter peak power (MW) | ~2 MW |
| Rx Antennas | E, W, V, S |

*Note*. IPP = interpulse period; Rx = receiver.

## 2. Experimental Technique

### 2.1. The 50-MHz Backscatter Radar Observations

The RTI map shown in Figure 1 is based on the 50-MHz Jicamarca ISR returns recorded during an MST-ISR-EEJ experiment on 17 April 2015. MST-ISR-EEJ is one of the observation modes used at Jicamarca for joint monitoring of the equatorial *D*, *E*, and *F* region ionospheres (e.g., Lehmacher et al., 2009) with a mix of MST, coherent backscatter, and ISR pulsing schemes. Data used for this study were sampled at 1-μs intervals matching the baud length of 64-baud complementary coded pulse pairs utilized in the MST mode having an interpulse period (IPP) of 202.5 km (or 1.35 ms) and average peak power of about 2 MW.

Table 1 presents a summary of the radar parameters used in the April 17, 2015, MST-ISR-EEJ experiment that utilized four radar beams, with the two-way radiation patterns shown in Figure 2—in the pattern plots the horizontal solid and dashed black lines represent the loci of perpendicularity to the geomagnetic field **B** for 100, 300, and 600 km of altitude computed using the 2015 IGRF model (e.g., Thébault et al., 2015), and the contour line thickness in each of the two-way radiation pattern contour lines is proportional to the antenna gain at −1, −3, −6, −9, −12, −15, −18, and −21 dB below the maximum beam gain.

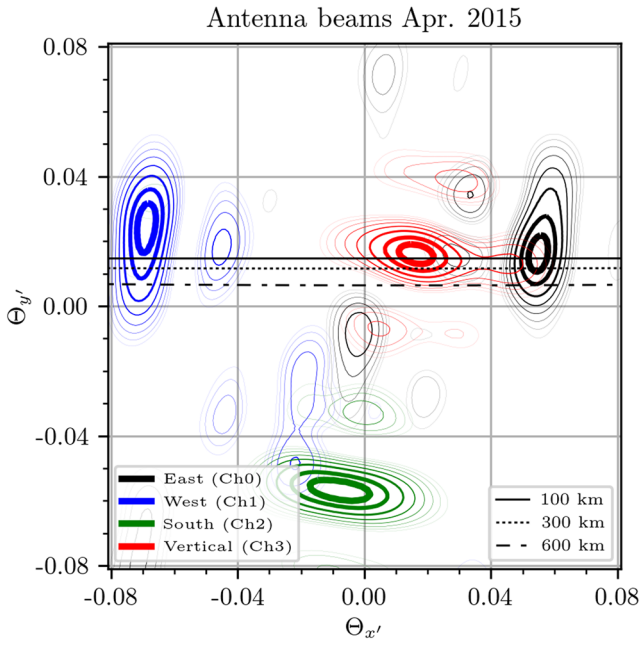


**Figure 2.** Contour plots of the two-way antenna beam patterns for the MST-ISR-EEJ campaign of April 2015. The figure shows superposed the contours of the two-way radiation patterns of the four beams used in the campaign plotted as a function of direction cosines $\Theta_{x'}$ and $\Theta_{y'}$ off the plane of the antenna array rotated in such a way that the loci of perpendicularity to the geomagnetic field **B** acquire horizontal orientations.

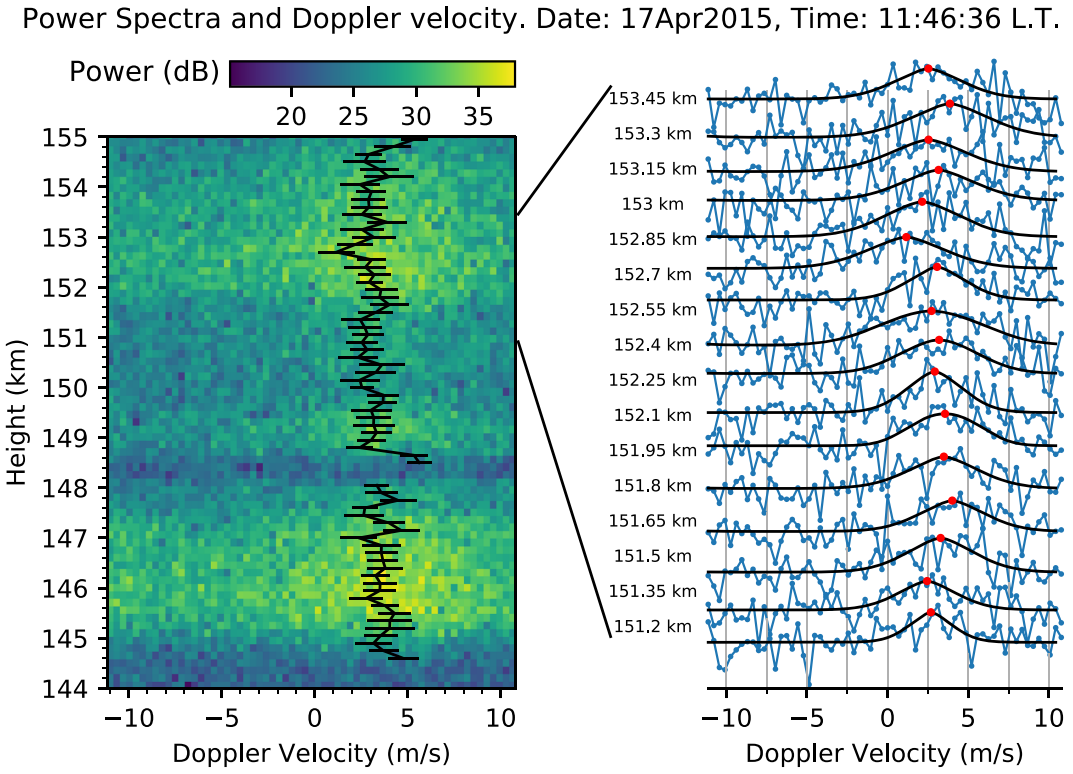


**Figure 3.** Power spectra and the Doppler velocity estimations and error bars for a minute-worth integrated data. This data were taken during an MST-ISR-EEJ campaign on 17 April 2015, around 11:46:36 local time with the vertical beam. The column on the left shows the spectra in dB as a color map with the Doppler velocity estimations as black lines with error bars. The right panel shows the individual power spectra in blue, the fitted model in black, and a red dot at the estimated Doppler shift for consecutive altitudes ranging from 151.2 to 153.45 km.

The MST mode backscatter data from 150-km region are processed as described by Kudeki and Fawcett (1993) to obtain Doppler spectrograms and make generalized Gaussian shaped spectral fits (e.g., Sheth et al., 2006) as shown in Figure 3. Vertical Doppler velocity estimates acquired in this manner can be used in Doppler velocity maps of 150-km echoes as shown in Figure 4—such Doppler velocity RTIs exhibit the

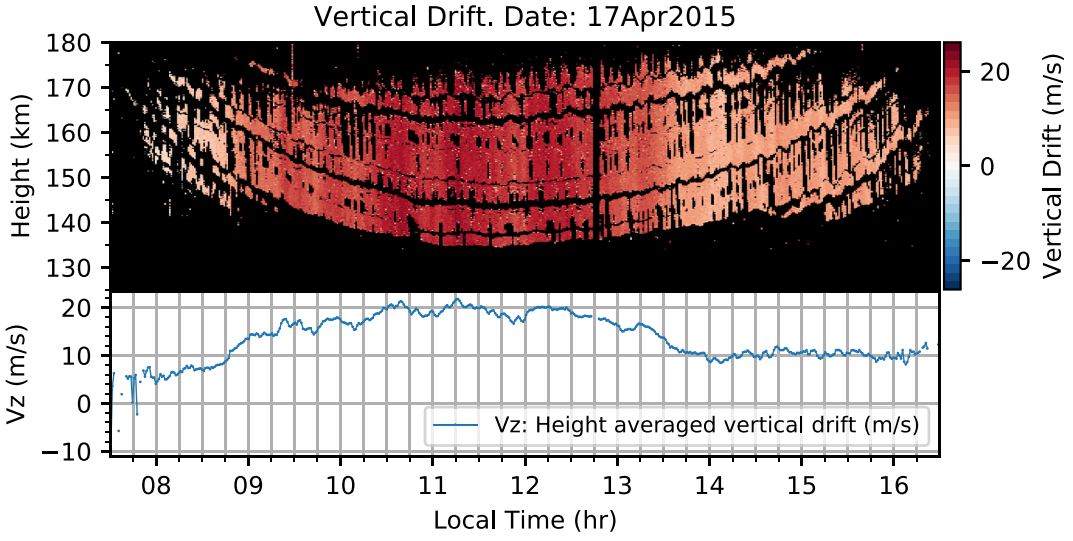


**Figure 4.** RTI of vertical **E×B** plasma drift from the 150-km region on the top and height averaged vertical drift on the bottom.

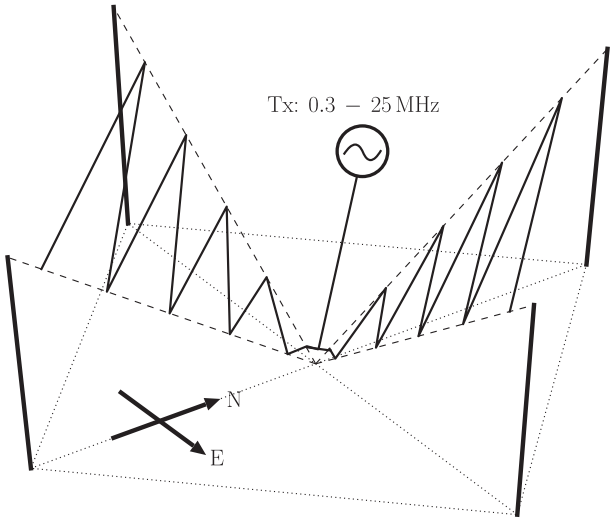


**Figure 5.** VIPIR transmitting wide-band antenna. Notice that this antenna configuration will produce a linearly polarized electric field in the northwest direction, exciting both ordinary (O) and extraordinary (X) modes of propagation.

general necklace shape of backscattered power RTIs similar to Figure 1. In constructing Figure 4, occurrences of frequency aliasing have been taken into account to correct the ±11.1 m/s Nyquist limit imposed by the data sampling period (see Table 1). The spectral analysis shows that on the day used in this study, 17 April 2015, the 150-km echoes observed are mostly of type NEIS.

### 2.2. VIPIR Observations

A "Vertical Incidence Pulsed Ionospheric Radar" unit known as VIPIR is located and operated at the Jicamarca Radio Observatory. This research grade ionosonde system is utilized in conjunction with the 50-MHz ISR system for purposes of probing diversity. The Jicamarca VIPIR system consists of a wide-band log-periodic antenna (see Figure 5) that transmits vertically propagating radio wave pulses by means of a 4-kW peak power transmitter capable of sweeping its frequency from 0.3 to 20 MHz.

VIPIR was configured in MST-ISR-EEJ experiments to transmit 70-μs-long (10.5 km) pulses with a raised cosine tapering. The transmission frequency was swept from 1.6 up to 12.5 MHz on a pulse-to-pulse basis over period of 10-s duration. The reflected pulses from the ionosphere are detected using eight short dipoles (see Figure 6) connected to eight coherent receivers. These receiving antennas form two orthogonal sets of interferometric baselines, in the northwest (NW) and northeast (NE) directions, which can be used jointly to detect the angle-of-arrival (AOA) of the reflected radio waves. The antennas in the NW baselines are polarized in the NW direction, just like NE baseline antennas are NE polarized. As a result, all eight receiving dipoles respond to both north-south polarized ordinary (O) and east-west polarized extraordinary mode (X) components of reflected VIPIR pulse returns, respectively.

Sample VIPIR ionograms are shown in Figure 7. Two ionograms shown on the top left in the figure correspond to the reflected power detected by Antennas 1 and 2 indicated in Figure 6, each including both ordinary (O) and extraordinary (X) mode returns forming separate power traces. The ionograms also show a set of quasi height-fixed horizontal interference bands at intervals of 200 km caused by MST-ISR-EEJ mode pulse transmissions of the nearby JRO ISR system. Two ionograms on top right represent an attempt to separate the O and X power traces of the ionograms on the left by using the sum and difference of the voltage outputs of Antennas 1 and 2, that is, as in

$$v_{O,X} = v_1 \pm g\, v_2, \tag{1}$$

including an adjustable complex valued gain factor $g$ close to 1 + j0—this is needed to account for possible phase and/or gain differences between the receivers of Antennas 1 and 2 as well as the magnetic declination angle variations with altitude. The derived ionograms corresponding to $\langle |v_O|^2 \rangle$ and $\langle |v_X|^2 \rangle$ are subsequently utilized to derive O- and X-mode virtual reflection height traces, which are displayed in the second row of Figure 7—the left two plots show the individual O and X traces superposed on O- and X- power curves whereas in the third plot, the O and X traces are shown with continuous and dashed lines, respectively.

Using only the O-mode traces, sampled at discrete frequencies and for all ionosonde observations taken in an extended experiment, one can form frequency-time-intensity (FTI) maps with the intensity indicating the O-mode virtual reflection height data as shown in the top panel of Figure 8. The center and bottom panels of the same

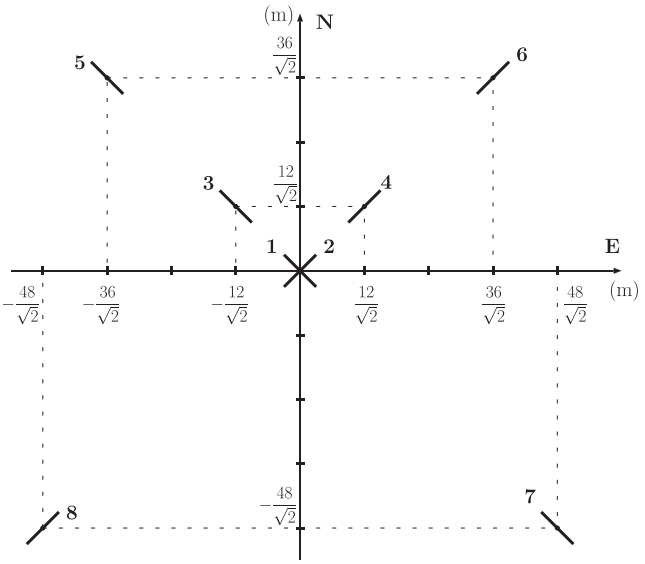


**Figure 6.** The diagram shows the location of the receiving antennas, which form two sets of orthogonal baselines. These antennas are oriented to be sensitive to both the ordinary (O) and the extraordinary (X) modes of propagation.

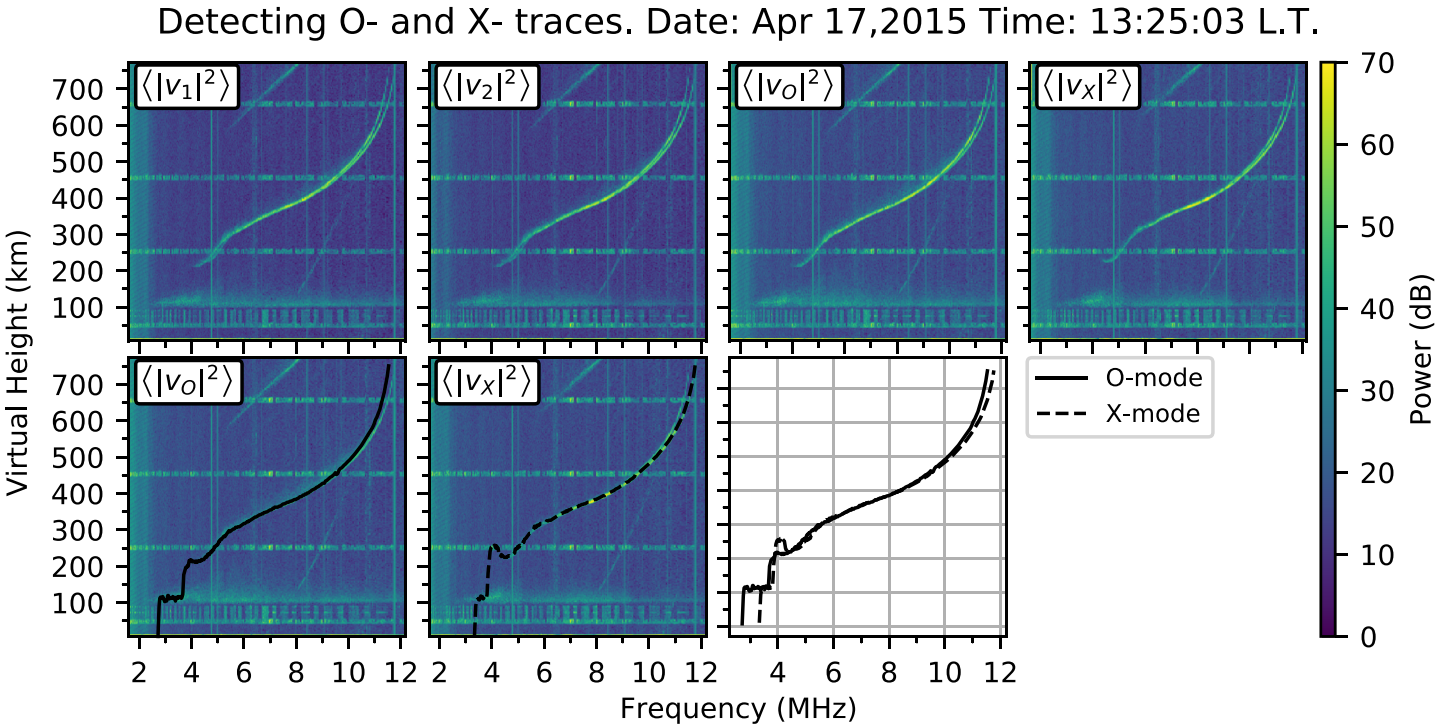


**Figure 7.** The ionograms in Columns 1 and 2 in the first row show the estimated power returns for Antennas 1 and 2, that is, $\langle|v_1|^2\rangle$ and $\langle|v_2|^2\rangle$. The plots in Columns 3 and 4 of the first row show the estimated power of O and X modes, $\langle|v_O|^2\rangle$ and $\langle|v_X|^2\rangle$. In the second row, $\langle|v_O|^2\rangle$ and $\langle|v_X|^2\rangle$ are plotted together with the estimated virtual height curves. The plot in Column 3, second row, shows the O and X traces of the ionogram.

figure depict FTI maps of AOAs estimated from the phase of the cross-correlation of spaced antenna outputs with the largest available separation baselines (84 m), namely, with the outputs of antenna pairs 5 and 7 for NW baselines and 6 and 8 for NE baselines.

In Figure 8 we notice that the VIPIR virtual heights and AOA data display oscillations with downward phase progressions. This is a very strong indication that the observed variations must be gravity wave induced since downward phase progression is a telltale sign of gravity wave propagation of energy and momentum from lower to higher altitudes in the upper atmosphere. We have made time series and scatter plots (shown in Figure 9) of sets of height averaged AOA data taken from the black and blue rectangles (near 2.94 and 9.69 MHz, respectively) shown in Figure 8. Scatter plots of the data sets seem to indicate that the reflection point of the ionosonde signal oscillated back and forth along an axis oriented in a fixed direction, implying gravity waves also propagating along the same direction. A systematic study of the valley region gravity waves detected by the Jicamarca VIPIR and 50-MHz ISR systems including the wave parameters (wavelengths, periods, and propagation directions) will be presented elsewhere.

## 3. ISR and VIPIR Data Comparisons

In section 2 we described RTI representations of the scattered power and Doppler velocity data obtained with the 50-MHz ISR system and FTI representation of VIPIR virtual height and AOA data. In this section our main focus will be on joint studies of these data maps.

Figure 10 shows in the top panel a VIPIR FTI map of O-mode virtual height data for 17 April 2015 and on the bottom panel a concurrent 50-MHz radar RTI plot of detected SNR for a radar beam pointing vertically, slightly off of perpendicular to Earth's magnetic field (radar beam pattern can be seen with red-colored contours in Figure 2). We notice that the thin "forbidden zone" layer undulations of the 150-km echoes shown in the RTI plot seem to coincide with the virtual height undulations shown in the FTI plot. One of these zones has in fact been highlighted with a red undulating line in the bottom panel and its height

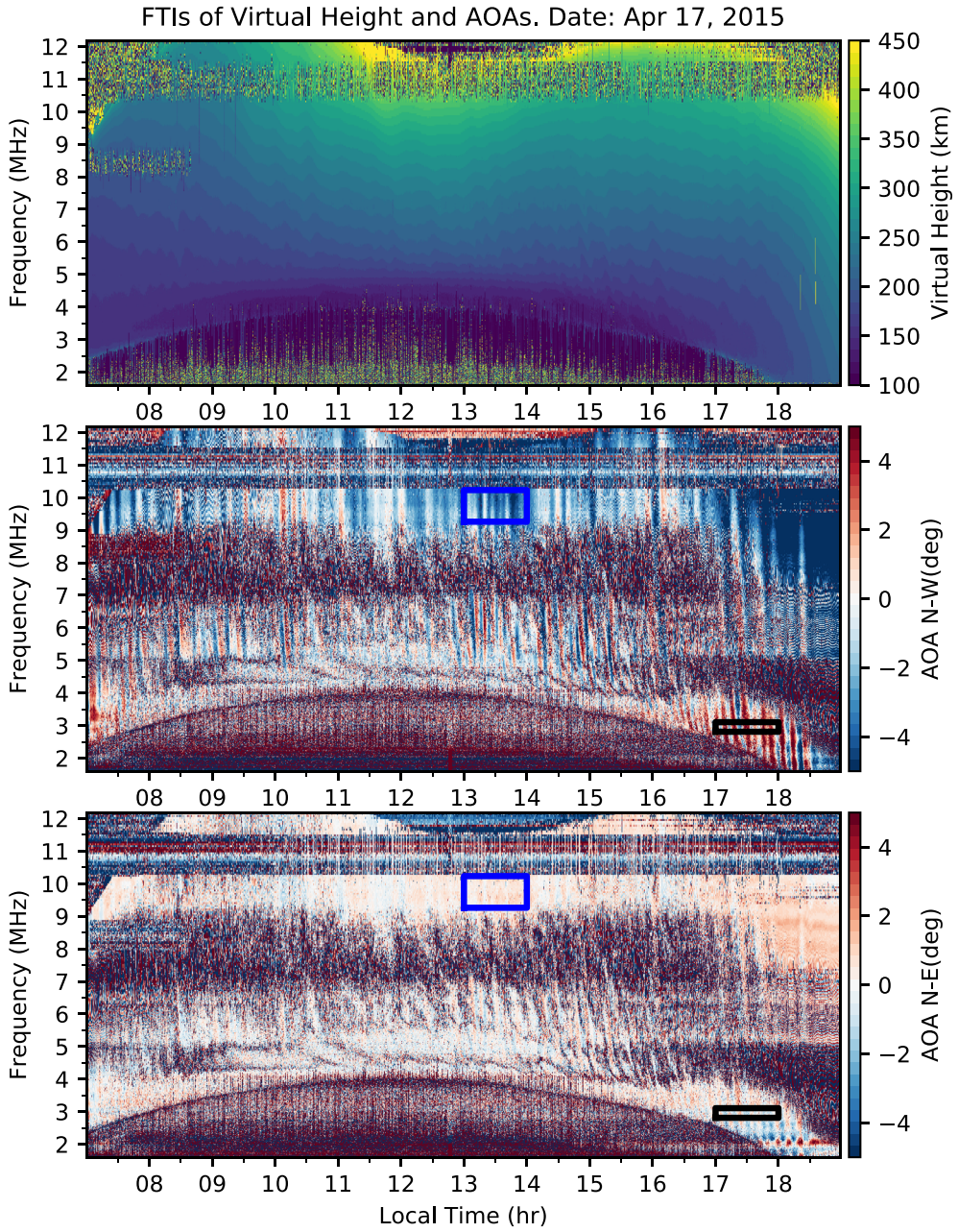


**Figure 8.** Frequency-time-intensity (FTI) plots. Top panel: ionosonde virtual reflecting height. Center panel: AOA of the reflected O-mode signal of the northwest interferometer. Bottom panel: same as center panel but for the northeast interferometer. The data were taken at JRO by the ionosonde VIPIR on 17 April 2015. The blue and black rectangles in the center and bottom panels indicate regions of strong AOA oscillations (see Figure 9).

information extracted as a time series to conduct quantitative comparisons with virtual height plots as described below—a portion of this highlighted forbidden zone can be seen as a red curve in a blow-up RTI in the left panel of Figure 11 where two other forbidden zone layers above and below are also traced with blue and magenta colored curves, respectively. The right panel of Figure 11 shows the detrended versions of these forbidden layer displacement heights. To detrend the displacement, a band-pass filter with cutoff frequencies 0.6 mHz (27.8 min) and 4 mHz (4.2 min) was used. The trend of the displacement height was obtained using a low-pass filter with cutoff frequency of 0.6 mHz (27.8 min) and is shown as yellow curves in the left panel of Figure 11.

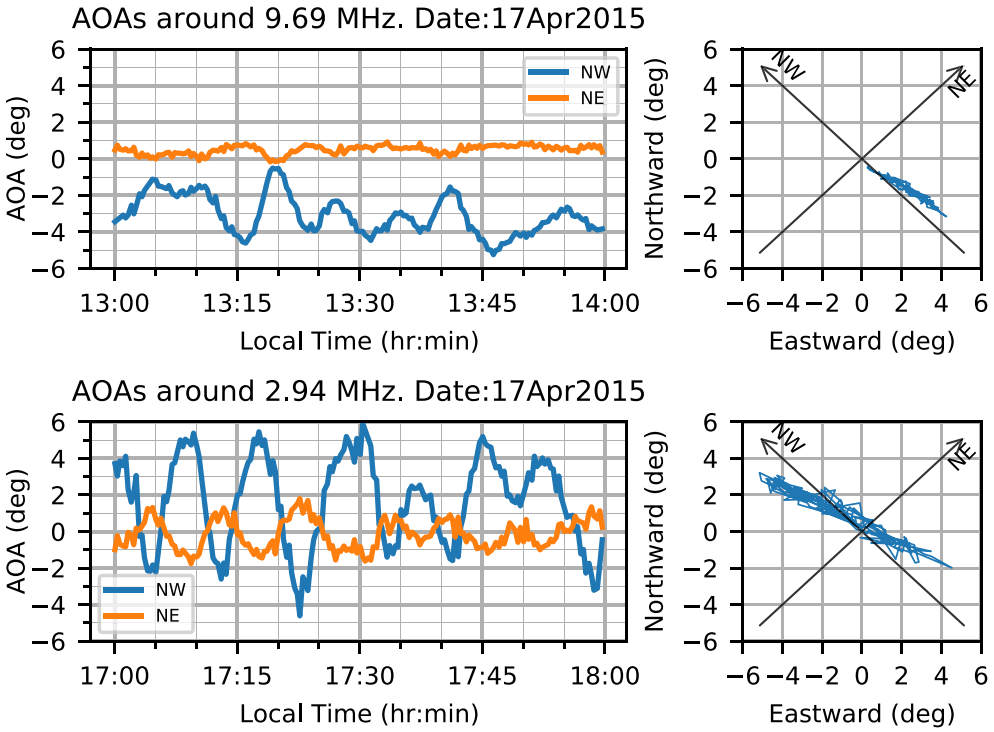


**Figure 9.** Time series and scatter plots of frequency averaged AOA data corresponding to the cuts indicated with blue (top panel) and black (bottom panel) rectangles in Figure 8. Scatter plots are aligned along the NW axis direction in both cases, corresponding to the propagation axis of gravity waves causing the AOA fluctuations.

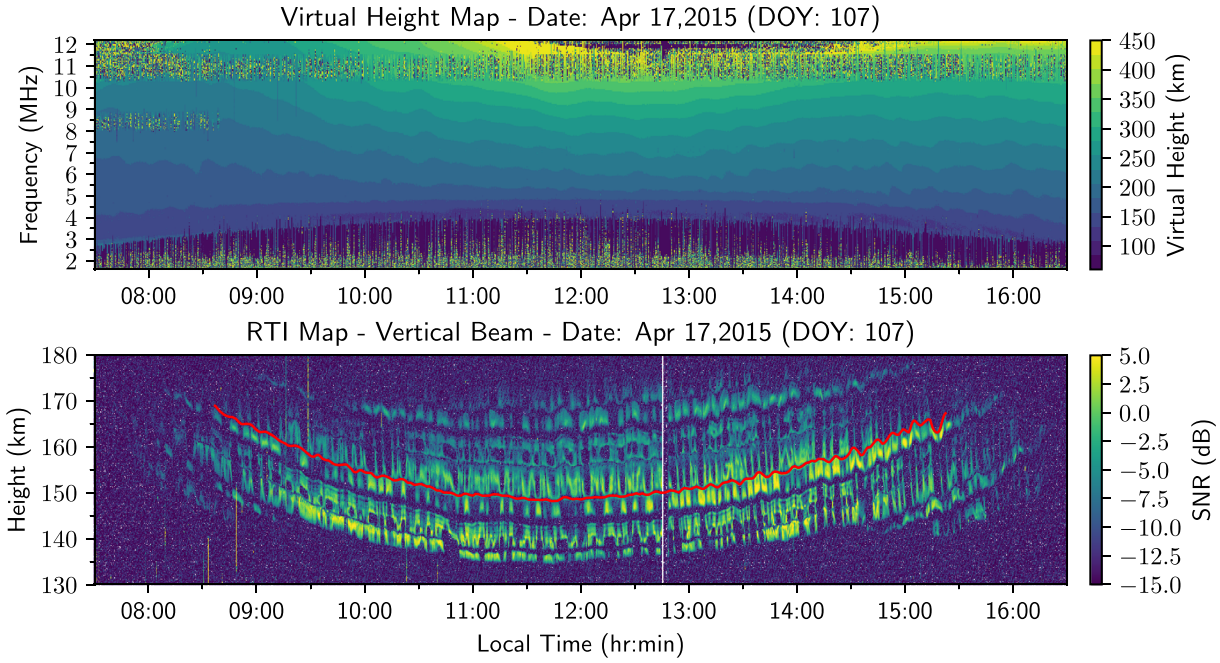


**Figure 10.** Top panel: VIPIR map depicting a frequency-time-intensity (FTI) plot of the virtual height of reflection of O-mode transmissions for 17 April 2015. Bottom panel: range-time-intensity (RTI) plot of signal-to-noise ratio (SNR) obtained at JRO using the MST-ISR-EEJ mode with a vertical pointing beam showing one of the "forbidden" thin layers highlighted with a red curve

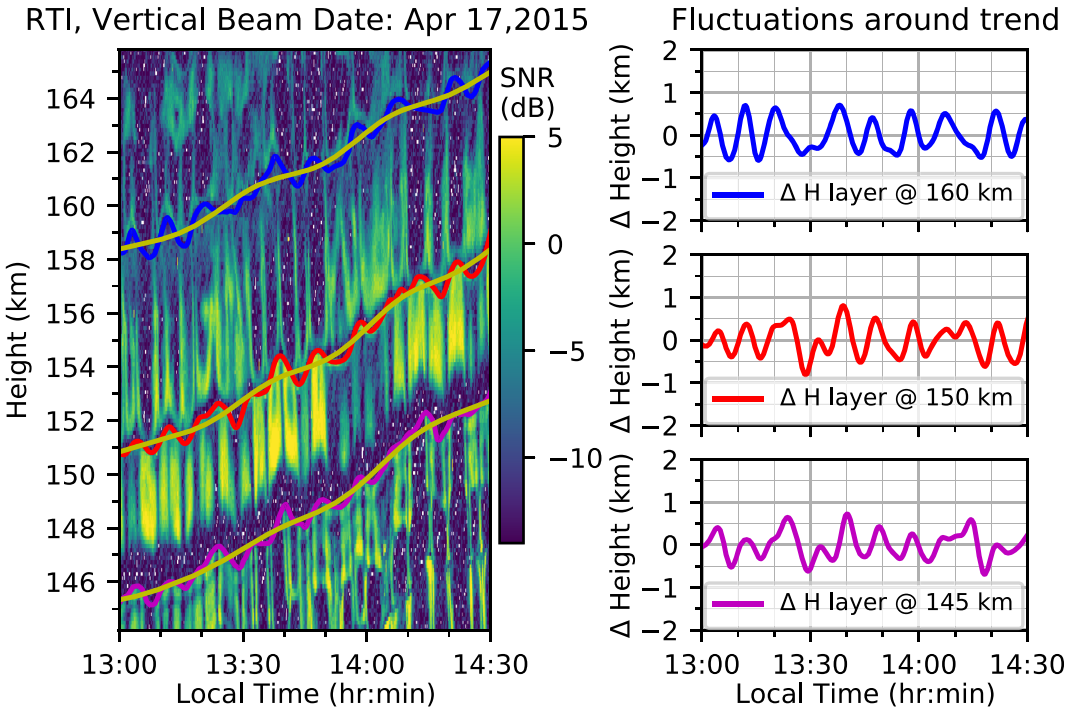


**Figure 11.** Left panel: RTI map showing three "forbidden" zone layers that have been highlighted with curves colored magenta, red, and blue. Right panel: plots of detrended versions of the forbidden layers versus time from the left panel. In the text, the magenta, red, and blue curves representing forbidden layers will be referred to as layers around @145, @150, and @160 km, respectively.

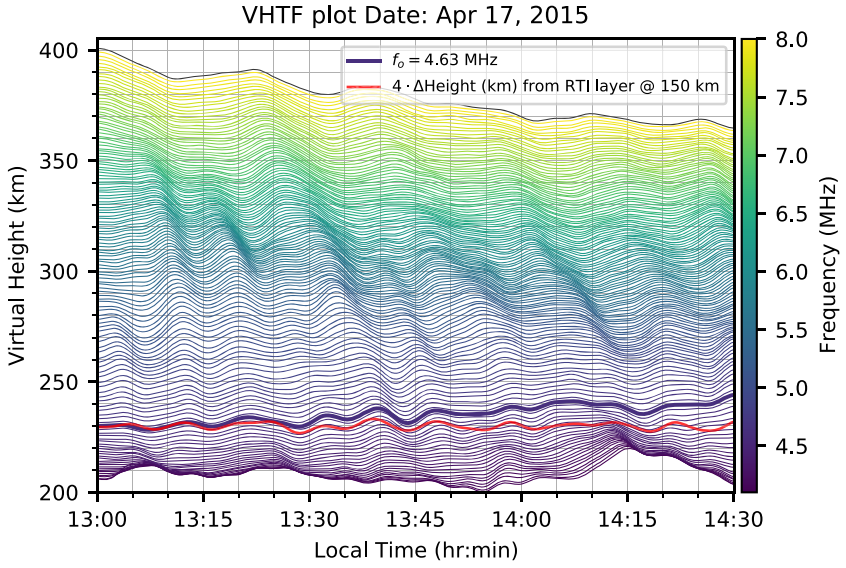


**Figure 12.** Representation of the O-mode virtual reflection height, transmission frequency, and observation time. The data represent a 1.5-hr segment of Figure 10. The thick red curve indicates a scaled-by-four curve taken from the 50-MHz RTI segment depicted in the right panel of Figure 11, referred to as @150 km, while the thick blue virtual height curve corresponding to 4.63-MHz transmission frequency has been highlighted. To obtain the O-mode virtual height curves, we followed the technique depicted in Figure 7, followed by the extraction of each individual O-trace curve and a manual correction if/when the algorithm failed.

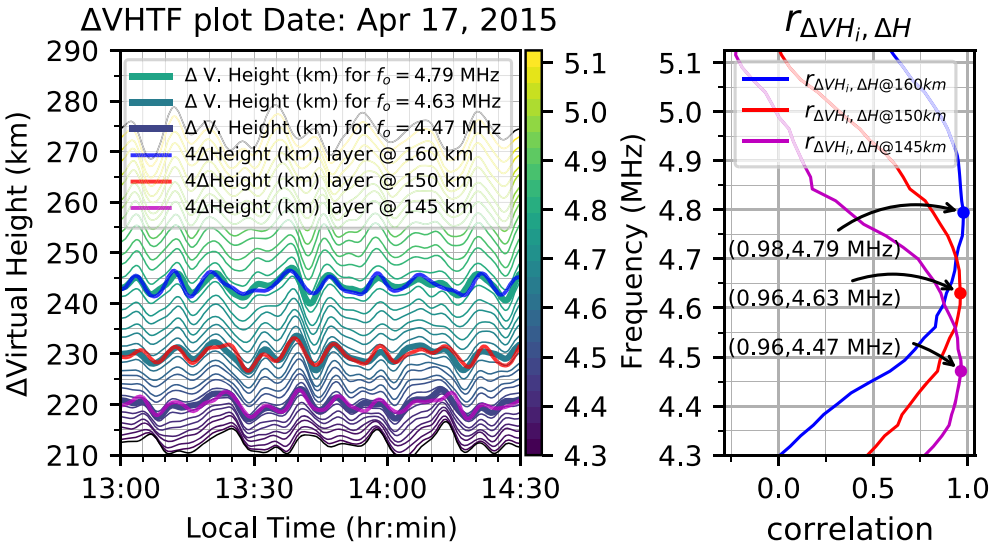


**Figure 13.** Left panel: a blow-up of Figure 12 with the virtual height curves detrended but preserving their initial virtual height. The thick magenta, red, and blue curves are scaled-by-four versions of the detrended 150-km echo layers from the right panel of Figure 11. Right panel: Each of the curves represents the normalized cross-correlation coefficients of each of the three detrended ΔH time series highlighted on the left panel with all the detrended virtual height ΔVH time-series of different plasma frequencies. The point of maximum cross-correlation for each curve is indicated with a dot along with its corresponding plasma frequency.

In Figure 12 we plot a dense set of virtual reflection height curves versus time, each curve colored by the frequency of reflection shown in the color bar. Ripples exhibiting downward phase progression in Figure 12 are signs of the distortion of ionospheric iso-density contours by propagating waves through the region. The rippling of the ionosphere is also evident in the AOA maps, for example, Figure 8, which show that reflections are not always coming from above; instead, they originate at the points where the line of sight starting from the antenna happens to be normal to space-time-modulated iso-density contour at the reflection instant. The observed modulations exhibit well-known characteristics of gravity waves, downward phase progression signatures as seen in Figure 12 for the virtual height, and in Figure 8 for the AOA; the implied vertical wavelengths and oscillation periods are all consistent with propagating gravity waves through the region with intrinsic periods just above the local Brunt-Väisälä period of about 10 min. Also, we see that some shorter wavelengths seen at lower altitudes are no longer seen at higher altitudes, which is known to happen due to viscosity.

More importantly for our analysis here, a red curve has been overlaid in Figure 12, representing the small-scale time variations of the "forbidden zone" displacement of 50-MHz backscatter shown in Figure 11 and establishing a direct link between the VIPIR ionosonde and VHF 150-km echo radar data. This detrended forbidden zone curve taken from the center plot in the right panel of Figure 11, representing real scattering heights centered about 155 km, best matched the virtual height variations depicted in Figure 12 at just about 230 km of virtual height and 4.63 MHz of plasma frequency corresponding to a plasma density of $2.66 \times 10^{11}$ m$^{-3}$, as a detrended blow-up of Figure 12 depicted in Figure 13 shows in further detail—the detrending of virtual height curves in Figure 13 has been done with the same bandpass filter used for the detrending of the 50-MHz 150-km echo layer. In both figures the overlaid forbidden zone height fluctuation curve was scaled up by a factor of 4 in order to match the amplitudes of virtual height fluctuations for 4.63-MHz reflections—this factor was obtained by manually adjusting it until the fluctuations of both instruments were of the same order. The best plasma frequency match for corresponding forbidden layers has been done by finding the largest correlation between the detrended layer oscillations from the radar ($\Delta H$) and the detrended virtual heights oscillations from VIPIR ($\Delta VH$) as shown in the right panel of Figure 13.

We will now turn our attention to comparisons of motion information extracted from the 50-MHz radar and VIPIR returns. Vertical $\mathbf{E} \times \mathbf{B}$ plasma drift velocity estimation from 50-MHz Doppler spectra measured

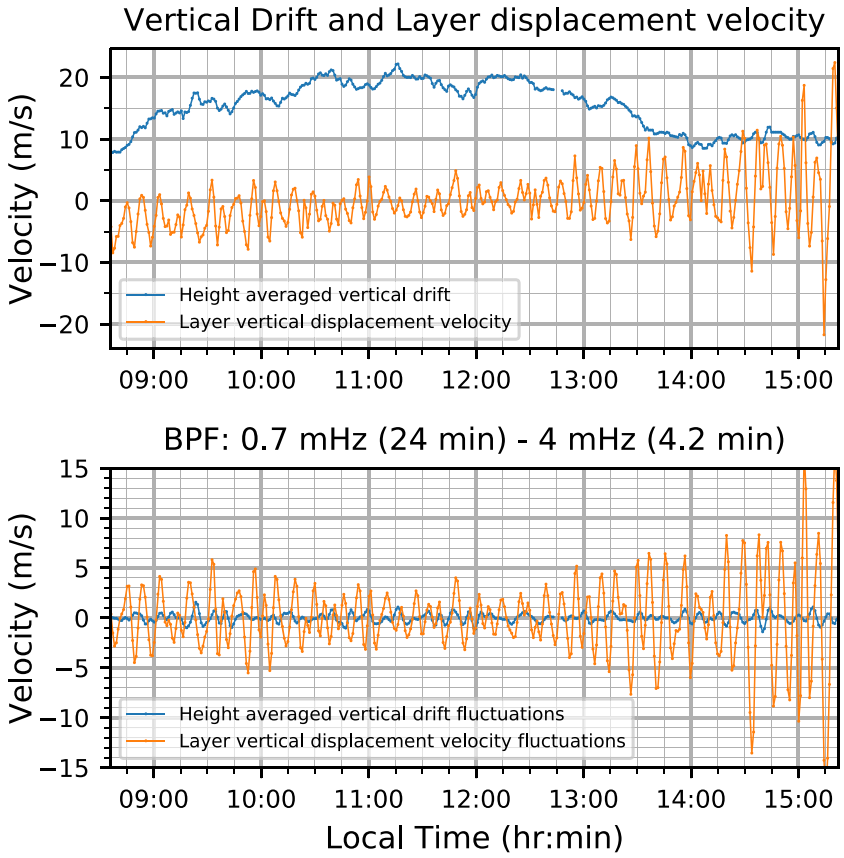


**Figure 14.** Top panel shows the vertical displacement velocity of the "forbidden" zone layer highlighted in Figure 10 together with vertical drift obtained by averaging ±5 km around the same layer. Bottom panel compares the fluctuations of the same signals from the top panel by filtering the signals with a band-pass filter with cutoff frequencies 0.7 mHz (24 min) and 4 mHz (4.2 min).

during MST-ISR-EEJ experiments was already described in section 2.1, where Figure 4 showed an RTI plot of vertical drifts for data taken on 17 April 2015. In Figure 14 we display the time series of the vertical drifts shown in Figure 4 averaged over an altitude band of 5-km width centered about the forbidden region height highlighted in Figure 10 by the red curve. Figure 14 also shows "vertical displacement velocities" obtained by differencing the forbidden region curve in Figure 10 before (top panel) and after (bottom panel) band-pass filtering it. Vertical displacement velocities (orange plots) shown in Figure 14 have about a few m/s fluctuation amplitudes while the Doppler fluctuation amplitudes (blue) within the same frequency band are very small, less than a m/s at all times. The measured broadband Doppler velocities of the 150-km signal returns shown in the upper panel of Figure 14 seem to be dominated by the upward $\mathbf{E}\times\mathbf{B}$ plasma motion observed in the region known to be driven by the global equatorial dynamo process. The displacement velocity of the forbidden layer and the adjacent scattering layers, on the other hand, seems to be unrelated to the upward $\mathbf{E}\times\mathbf{B}$ drift of the plasma in the region and has a by and large zero-mean oscillatory nature with oscillation amplitudes far greater than the oscillatory component observed in the Doppler velocity data. In fact, the oscillatory component of the observed Doppler velocity is so weak that it is not surprising, in retrospect, why previous papers on 150-km echoes make no mention of this component.

## 4. Discussion and Conclusions

We have presented Jicamarca 50-MHz radar and VIPIR ionosonde data taken in high-resolution and high-sensitivity modes to study the dynamics and fluctuations of the 150-km echoing region. The 50-MHz

radar data enable the construction of high-resolution backscattered power and line-of-sight Doppler velocity maps (RTI plots of power and Doppler velocity) exhibiting the intricate necklace shapes reported in earlier work from Jicamarca. VIPIR ionosonde data enable the construction of virtual reflection height maps (FTI plots) with fluctuations well matching the intricate fluctuations observed in the necklace-shaped 50-MHz backscattered power maps. Matching specific features of the FTI and RTI maps, we have been able to assign true height data to selected pairs of ionosonde reflection frequency and virtual reflection height data within the valley region of the equatorial ionosphere centered about 150-km altitude. "Height calibrated" VIPIR maps obtained in this manner show that the entire daytime valley region is continually modulated by propagating gravity waves through the region. This conclusion is deduced from the downward phase progression of the fluctuating features of VIPIR FTI maps as well as h′TI maps (virtual height time intensity maps) of VIPIR reflection frequencies.

This gravity wave modulation of the valley region ionosphere (deduced from height calibrated VIPIR data) appears to be directly responsible for the short time scale (11-min) oscillations of the layered 50-MHz backscatter power returns portrayed in the necklace-shaped power RTI maps. The oscillations of what we have called forbidden layers in this paper, thin regions devoid of any significant 50-MHz backscatter, immediately adjacent to intensely echoing regions would also be caused by the same wave dynamics. We still do not know the exact physical mechanism of wave enhancement and suppression of backscattering giving rise to the observed echoing and forbidden layers, but the present observations (and many more data of similar type presented in Lehmacher et al., 2020) already indicate that the mechanism must be electron density controlled as the gravity wave-induced ripplings of iso-density contours of the ionosphere probed by the VIPIR instrument *match* the fluctuations and ripplings observed in the 50-MHz backscattered power data with very high fidelity. An electron density-dependent resonance condition—either of a field-aligned configurational nature or else an intrinsic resonance of a magnetized plasma, such as upper hybrid resonance (e.g., Longley et al., 2020)—remains as a plausible candidate to explain the observations, an idea that we need to explore via modeling studies. While in this paper we have presented data collected during a single day of observation, a similar analysis of a broader data set collected over many years and seasons is reported in Lehmacher et al. (2020) with a focus on the occurrence conditions of forbidden layers introduced in this paper.

We have also investigated in this work the relationship between 150-km echo Doppler velocities and velocities corresponding to vertical displacements of 150-km echoing and forbidden layers. While the scattering layers are by and large moved by zero-mean oscillatory velocities of a few m/s amplitudes, the measured Doppler velocities corresponding to the motion of Bragg-scale wave packets of plasma density are dominated by slowly varying nonzero means corresponding to dynamo-driven $\mathbf{E}\times\mathbf{B}$ drift velocity of the plasma in the region and contain barely detectable levels of a fluctuating component at the same period of the layer velocity oscillations.

An interpretation of these observations is as follows: Bragg-scale electron density wave packets backscattering the 50-MHz radar transmissions appear to be moving with the vertical bulk motion of the plasma (the flow pattern in the equatorial fountain) in and out of undulating layers where their amplitudes are enhanced and suppressed (forbidden regions) in succession, layers that in turn appear to be moving up and down periodically with a few m/s velocity amplitudes and about 10-min periods. If layers of enhancements and suppression correspond to isodensity layers as we have argued for earlier in this section, and yet if the same layers are not displaced continually with the bulk plasma motion of the region, as our velocity comparisons seem to indicate, we are then led to conclude that the plasma in the region does not behave as a "passive scalar"—that is, the structure of the plasma density variations must be dominated by photochemistry rather than simple electrodynamics in the region (which is hardly surprising in the production region of the ionosphere at these altitudes), and gravity wave-induced structure modulations must not be caused by wave-generated perturbation electric fields, for otherwise the oscillation amplitudes would have been equal for the layer displacements and measured Doppler velocities. Negligible levels of Doppler velocity oscillations detected at the same periods as the layer displacements is a strong indication that gravity wave-driven $\vec{\delta} V \times \vec{B}$ perturbation fields must be shorted out, by and large, by field-aligned currents closing across low impedance paths in the region. In the absence of the $\vec{\delta} V \times \vec{B}$ polarization field, we may conjecture that what transports the plasma, giving rise to the rippling effect of isodensity contours seen in VIPIR

FTI maps, must be related to field-aligned wind forcing by the meridional component of wave-related wind perturbations.

The "observed" shorting of gravity wave $\vec{\delta} V \times \vec{B}$ forcing of the valley region plasma, discussed above, may in fact be an essential feature of the excitation mechanisms of scattering and forbidden layers seen in RTI maps. Field-aligned shorting is only possible in the presence of field-aligned currents that are likely to have some role in the enhancement or destabilization or even suppression of naturally occurring Bragg-scale density irregularities seen by the radar, depending on direction and relative phases. The role of field-aligned currents on (possibly) photoelectron-enhanced density waves is yet another mechanism that needs attention in future modeling studies of 150-km physics.

From an experimental perspective, further combined VIPIR and 50-MHz radar observations, with the 50-MHz radar operated as an ISR probe of the valley region ionosphere, should continue to provide useful hints about the pertinent processes for 150-km echo generation. Determination of gravity wave parameters and amplitudes, as well as joint inversions of VIPIR and valley region ISR data for the true height distribution of valley region electron densities in and around the enhanced and forbidden 150-km echo layers, are high-priority experimental steps that need immediate attention.

## Data Availability Statement

The radar and VIPIR data as well as the code used to generate the figures are available in the OSF public repository (DOI: https://doi.org/10.17605/OSF.IO/2FKA6).

**Acknowledgments**

E. Kudeki and P. Reyes were supported by NSF Grant AGS-1143523. G. Lehmacher was supported by NSF Grant AGS-1143514. Jicamarca is a facility of the Instituto Geofísico del Perú operated with support from the NSF Grant AGS-1433968 through Cornell University. We thank the Jicamarca staff for supporting the MST-ISR and MST-EEJ-ISR experiments. The participation of J. L. C. in this work is part of the project supported by the Deutsche Forschungsgemeinschaft (DFG, German Research Foundation) under SPP 1788 (DynamicEarth)-CH 1482/1-2 (DYNAMITE2). We thank the International Space Science Institute for facilitating discussions related to this paper as part of the International Team "An Exploration of the Valley Region in the Low Latitude Ionosphere: Response to Forcing from Below and Above and Relevance to Space Weather".

## References

Balsley, B. B. (1964). Evidence of a stratified echoing region at 150 kilometers in the vicinity of the magnetic equator during daylight hours. *Journal of Geophysical Research*, *69*(9), 1925–1930. https://doi.org/10.1029/JZ069i009p01925

Chau, J. L., & Kudeki, E. (2013). Discovery of two distinct types of equatorial 150 km radar echoes. *Geophysical Research Letters*, *40*, 4509–4514. https://doi.org/10.1002/grl.50893

Chau, J. L., & Woodman, R. F. (2004). Daytime vertical and zonal velocities from 150-km echoes: Their relevance to *F*-region dynamics. *Geophysical Research Letters*, *31*, L17801. https://doi.org/10.1029/2004GL020800

Chau, J. L., Woodman, R. F., Milla, M. A., & Kudeki, E. (2009). Naturally enhanced ion-line spectra around the equatorial 150-km region. *Annales Geophysicae*, *27*(3), 933–942. https://doi.org/10.5194/angeo-27-933-2009

Kudeki, E., & Fawcett, C. D. (1993). High resolution observations of 150 km echoes at Jicamarca. *Geophysical Research Letters*, *20*(18), 1987–1990. https://doi.org/10.1029/1998GL900069

Kudeki, E., Fawcett, C. D., Ecklund, W. L., Johnston, P. E., & Franke, S. J. (1998). Equatorial 150-km irregularities observed at Pohnpei. *Geophysical Research Letters*, *25*(21), 4079–4082. https://doi.org/10.1029/93GL01256

Lehmacher, G. A., Kudeki, E., Akgiray, A. H., Guo, L., Reyes, P. M., & Chau, J. L.(2009). Radar cross sections for mesospheric echoes at Jicamarca. *Annales Geophysicae*, *27*(7), 2675–2684. https://doi.org/10.5194/angeo-27-2675-2009

Lehmacher, G. A., Wu, H., Kudeki, E., Reyes, P. M., Hysell, D. L., & Milla, M. (2020). Height variation of gaps in 150-km echoes and whole atmosphere community climate model electron densities suggest link to upper hybrid resonance. *Journal of Geophysical Research: Space Physics*, *125*, e2019JA027204. https://doi.org/10.1029/2019JA027204

Longley, W. J., Oppenheim, M. M., Pedatella, N. M., & Dimant, Y. S. (2020). The photoelectron-driven upper hybrid instability as the cause of 150-km echoes. *Geophysical Research Letters*, *47*, e2020GL087391. https://doi.org/10.1029/2020GL087391

Oppenheim, M. M., & Dimant, Y. S. (2016). Photoelectron-induced waves: A likely source of 150 km radar echoes and enhanced electron modes. *Geophysical Research Letters*, *43*, 3637–3644. https://doi.org/10.1002/2016GL068179

Patra, A. K., & Rao, N. V. (2006). Radar observations of daytime 150-km echoes from outside the equatorial electrojet belt over Gadanki. *Geophysical Research Letters*, *33*, L03104. https://doi.org/10.1029/2005GL024564

Patra, A. K., & Rao, N. V. (2007). Further investigations of 150-km echoing riddle using simultaneous observations of 150-km and *E* region echoes from off-electrojet location Gadanki. *Journal of Geophysical Research*, *112*, A09301. https://doi.org/10.1029/2006JA012204

Patra, A. K., Yokoyama, T., Otsuka, Y., & Yamamoto, M. (2008). Daytime 150-km echoes observed with the Equatorial Atmosphere Radar in Indonesia: First results. *Geophysical Research Letters*, *35*, L06101. https://doi.org/10.1029/2007GL033130

Reyes, P. M. (2012). Solar-flare effects observed over Jicamarca during MST-ISR experiments (Master's Thesis), Urbana, Illinois. http://hdl.handle.net/2142/31196

Rodrigues, F. S., De Paula, E. R., & Chau, J. L. (2011). On the characteristics of 150-km echoes observed in the Brazilian longitude sector by the 30 MHz São Luís radar. *Annales Geophysicae*, *29*(10), 1905–1916. https://doi.org/10.5194/angeo-29-1905-2011

Sheth, R., Kudeki, E., Lehmacher, G. A., Sarango, M. F., Woodman, R. F., Chau, J. L., et al. (2006). A high-resolution study of mesospheric fine structure with the Jicamarca MST radar. *Annales Geophysicae*, *24*(5), 1281–1293. https://doi.org/10.5194/angeo-24-1281-2006

Thébault, E., Finlay, C., Beggan, C., Alken, P., Aubert, J., Barrois, O., et al. (2015). International geomagnetic reference field: The 12th generation. *Earth, Planets and Space*, *67*(1), 79. https://doi.org/10.1186/s40623-015-0228-9

Tsunoda, R. T., & Ecklund, W. L. (2000). On the nature of 150-km radar echoes over the magnetic dip equator. *Geophysical Research Letters*, *27*(5), 657–660. https://doi.org/10.1029/2007GL032152

Tsunoda, R. T., & Ecklund, W. L. (2008). On the sheet like nature of 150-km ($F_1$) radar echoes. *Geophysical Research Letters*, *35*(5), L05102. https://doi.org/10.1029/1999GL003689

Yokoyama, T., Hysell, D. L., Patra, A. K., Otsuka, Y., & Yamamoto, M. (2009). Zonal asymmetry of daytime 150-km echoes observed by Equatorial Atmosphere Radar in Indonesia. *Annales Geophysicae*, *27*(3), 967–974. https://doi.org/10.5194/angeo-27-967-2009